ARTICLES

Ground and Excited State Hydrogen Atom Transfer Reactions and Cyclization of 2-Acetylbenzoic Acid

L. Santos,[†] A. Vargas,[‡] M. Moreno,*[,§] B. R. Manzano,[||] J. M. Lluch,[§] and A. Douhal*[,‡]

Departamento de Química-Física, Facultad de Ciencias Químicas, Universidad de Castilla-La Mancha, 13071 Ciudad Real, Spain, Departamento de Química-Física, Sección de Químicas, Facultad de Ciencias del Medio Ambiente, Universidad de Castilla-La Mancha, Avenida Carlos III, S.N. 45071, Toledo, Spain, Departament de Química, Facultat de Ciències, Universitat Autónoma de Barcelona, 08193 Bellaterra, Barcelona, Spain, Departamento de Química Inorgánica, Orgánica y Bioquímica, Facultad de Ciencias Químicas, Universidad de Castilla-La Mancha, 13071 Ciudad Real, Spain

Received: April 16, 2004; In Final Form: July 9, 2004

We present experimental and theoretical studies of the ring−chain tautomerism (H-atom transfer and cyclization) for 2-acetylbenzoic acid at both ground and electronically first excited states. ^{1}H and ^{13}C NMR studies in solution confirm the existence of equilibrium between the open and ring structures at the ground state, with the ring one being dominant (∼90%). Temperature-dependent ^{1}H NMR experiments allowed obtaining the thermodynamic and kinetic parameters at the coalescence temperature (380 K). Fluorescence measurements disclose the involvement of highly efficient nonradiative processes in agreement with the theoretical data. Electronic calculations for the ground state give additional information on the different conformers of the open tautomer. In agreement with the experiment the most stable structure is of the closed ring tautomer, and it is obtained after additional internal rotations of the −COOH and −CO(CH_3) fragments. Intrinsic reaction coordinate calculations indicate that the ring formation/breaking and the H-atom transfer are taking place in a concerted but not synchronous manner. At S_1 the most stable form is the open one, for which different conformers are also found. The influence of the solvent is also accounted for through a model that considers the solvent as a continuum at both the ground and excited electronic states. No major differences were observed when comparing both gas and condensed phase results, so calculations of the isolated molecule should give a picture of the reaction which is experimentally observed in solution.

1. Introduction

In molecules bearing both proton (or hydrogen atom) donor and acceptor groups, an intramolecular hydrogen bond is generally formed and observed when the involved groups are in suitable positions.[1] Thermal or photonic activation of these systems may lead to a proton (or hydrogen atom) transfer reaction and thus produces new products. Therefore, great effort has been made for a better understanding and control of this reaction. The phenomenon of ring−chain tautomerism[2] is also possible and plays an important role in many aspects of chemistry and biology.[3,4] Such tautomerism has been shown to occur in a number of oxocarboxylic acids giving rise to both closed (ring) and open (chain) forms. Molecules showing this kind of reaction can be used as starting materials for potential use in nanotechnology such as molecular memories. In this work, we will focus on 2-acetylbenzoic acid (AB), a molecule which exhibits such a reaction (Scheme 1).

SCHEME 1

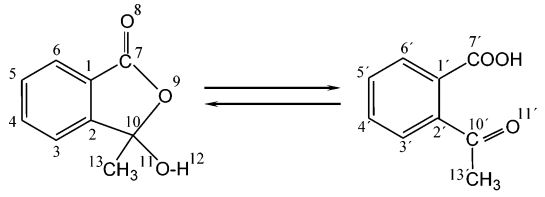

Ring Form Open Form

The whole reaction implies a rearrangement in which the acid hydrogen atom (H_{12}) migrates from the carboxylic group to the acetyl one. The process yields the formation of a new C−O bond so that an additional ring is formed. The dynamics and issues of this kind of reaction are determined by the shape of the multidimensional potential energy surface (PES).[1,5] Surprisingly, little work on the ring−chain tautomerism of oxocarboxylic acids has been reported.[6−9] Experimental determination of the equilibrium constant for the ring−chain tautomeric equilibrium was done by Finkelstein et al.[6] They obtained the UV−IR absorption spectra and also the ^{1}H NMR spectra of 2-acetylbenzoic acid (and of some 6-derivatives), concluding

* Corresponding authors. Fax: +34-925-268840. E-mail: abderrazzak.douhal@uclm.es (A.D.); Miquel.Moreno@uab.es (M.M.).

[†] Departamento de Química-Física, Facultad de Ciencias Químicas, Universidad de Castilla-La Mancha.

[‡] Departamento de Química-Física, Sección de Químicas, Facultad de Ciencias del Medio Ambiente, Universidad de Castilla-La Mancha.

[§] Universitat Autónoma de Barcelona.

[||] Departamento de Química Inorgánica, Orgánica y Bioquímica, Facultad de Ciencias Químicas, Universidad de Castilla-La Mancha.

10.1021/jp048330j CCC: $27.50
Published on Web 10/02/2004

that the ring tautomer is the dominant form. The IR and ^{1}H NMR spectra of the same molecule were also reported by Bowden and Taylor.[7a] Their results agree with the previous one and show that the closed structure is the dominant one. The relative populations of both tautomers and their equilibrium constants depend on the experimental conditions (nature of the solvent and the initial concentration of the 2-acetylbenzoic acid). The structure of AB was studied by X-ray diffraction, and it corresponds to the phthalide (ring) form.[8] The intermolecular bond in the crystal is made up of only one type of hydrogen bond formed between the hydrogen-12 of one molecule and oxygen-8 of the carbonyl group of the neighboring molecule (Scheme 1).

More recently, Fabian and co-workers have carried out a theoretical work on the subject.[9] They restricted the study to the relative stability of the two tautomers and analyzed the possible conformers that result from rotations around the $C'_1-C'_7$ and $C'_2-C'_{10}$ single bonds in the open form (Scheme 1). The calculations were performed at several ab initio and DFT levels of theory, and the solvent effect was also included by means of a continuum method by using the dielectric constant of water. Their results, in terms of Gibbs free energy differences, fail to reproduce the experimental observations as one of the open conformations was always the most stable structure in the gas phase. However, upon introduction of the solvent effect, the stability pattern was reversed and the ring tautomer became the lowest energy structure in water solution.

The purpose of this work is to analyze the mechanism of the ring−chain tautomerism of 2-acetylbenzoic acid. Therefore, results of experiments devoted to evaluating not only the equilibrium constant but also the kinetic parameters of the reaction are presented. From the theoretical point of view, calculations were done to analyze the potential energy change in order to understand the mechanism of such a reaction. Molecules related to 2-acetylbenzoic acid such as the derivatives of salicylic acid have recently been the focus of attention because upon irradiation the difference in stability of the different tautomers makes these molecules potential material for optical memories.[10] In this sense, we have not restricted the study of 2-acetylbenzoic acid to the ground electronic state, but we have also analyzed the first singlet excited electronic state behavior. Given that experiments are carried out in liquid phase, the solvent effect is also accounted for through the use of a continuum model.

2. Experimental and Theoretical Details

2.1. Experimental Section. 2-Acetylbenzoic acid (Sigma-Aldrich, >99%) was sublimed and recrystallized in cyclohexane, and its purity was checked and confirmed by fluorescence spectroscopy. Sigma-Aldrich (>99%) solvents were spectrograde. Absorption and emission spectra were recorded on Varian (Cary E1) and Perkin-Elmer (LS-50B) spectrophotometers, respectively. ^{1}H and ^{13}C{^{1}H} NMR spectra ($CDCl_3$ or DMSO-d_6) were recorded on a Varian Unity 300 spectrometer. Chemical shifts (ppm) are given relative to TMS. Coupling constants are given in hertz. ^{1}H−^{13}C COSY spectrum was produced with a standard pulse sequence with an acquisition time of 0.076 s, a pulse width of 90°, a relaxation delay of 1 s, number of scans of 20, and number of increments of 160. For variable temperature spectra the probe temperature (±1 K) was controlled by a standard unit calibrated with a methanol reference.

2.2. Theoretical Calculations. Ab initio calculations have been performed using the Gaussian 98 series of programs.[11] The S_0 state has been studied using the B3LYP density functional approach.[12,13] For the excited S_1 state, a configuration interaction all-single-excitations with a spin-restricted Hartree−Fock reference ground state (CIS) has been used to optimize geometries.[14] Single point energies of the excited state have also been calculated by the time-dependent formalism within the B3LYP functional (TD-DFT (density functional theory) calculations).[15] All calculations have been done with the split-valence 6-31+G(d) basis set, which includes a set of d polarization functions and a set of sp diffuse functions on atoms other than hydrogens.[16] For comparative purposes, we have also used the complete active space self-consistent field method (CASSCF)[17] to optimize the geometries in both the ground and the excited electronic states.

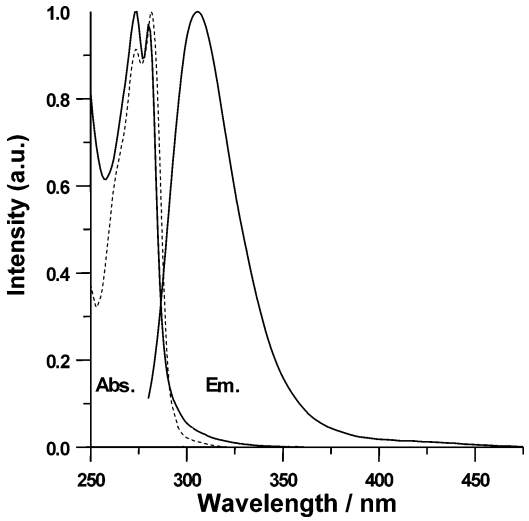

Figure 1. Room-temperature UV−visible absorption (Abs.) and emission (Em., $\lambda_{ex.}$ = 260 nm) (—) spectra of 2-acetylbenzoic acid (AB) in methanol. Excitation spectrum (---) of AB in methanol for λ_{obs} = 350 nm.

Full geometric optimization and direct location of stationary points (minima and transition states) have been carried out by means of the Schlegel gradient optimization algorithm[18] by using redundant internal coordinates as implemented in the Gaussian 98 package.[11] Diagonalization of the energy second-derivative matrix has been performed to disclose the nature of each stationary point: no negative eigenvalues indicate a minimum whereas one negative eigenvalue identifies a transition state. To establish the connection between the transition states and the corresponding equilibrium structures, the reaction pathways were followed using the intrinsic reaction coordinate procedure (IRC).[19] Diagonalization of the second-derivative matrix also provides the vibrational harmonic frequencies that were used for evaluating the thermodynamic corrections at 1 atm and 298.15 K to the initially obtained electronic energy by using the standard statistical formulas, assuming that the system behaves as an ideal gas and that the rotational and vibrational degrees of freedom are well described through the rigid rotor and harmonic approximations, respectively.[20] The bulk effect of the solvent has been introduced through the isodensity surface polarized continuum model (IPCM).[21] We have used an electronic density of 0.0005 au to define the cavity in this model. The IPCM calculations have been carried out both in S_0 and S_1 without reoptimization of the geometries.

3. Results and Discussion

3.1. Experimental Results. AB is very poorly soluble in apolar solvents, so the experiment has been done in a polar medium. Therefore, in methanol (Figure 1) the molecule shows

TABLE 1: Values of Free Energy of Activation for the Ring ↔ Chain Transformation of AB in 1,1′,2,2′-Tetrachloroethene-d_2 and of Other Parameters Deduced from NMR Experiment (See Text)

T_c[a]	P_O[b]	P_R[c]	$\delta\nu$[d]	$k_{R\rightarrow O}$[e]	$k_{O\rightarrow R}$[f]	$\Delta G^{\circ\#}_{(R\rightarrow O)}$[g]	$\Delta G^{\circ\#}_{(O\rightarrow R)}$[h]
380	0.18	0.82	195	93	408	19	18

[a] Coalescence temperature in K. [b] Relative population of the open form. [c] Relative population of the ring form. [d] Difference in chemical shift (in Hz) between the open and ring forms. [e] Rate constant (in s^{-1}) for the ring → open reaction. [f] Rate constant (in s^{-1}) for the open → ring reaction. [g] Gibbs free energy of activation (in kcal/mol) for the ring → open reaction. [h] Gibbs free energy of activation (in kcal/mol) for the open → ring reaction.

a structured UV absorption band with peaks at 278 and 282 nm, a result that agrees with the findings of Finkelstein et al.[6] However, we found that this molecule has a very small emission quantum yield ($<10^{-5}$), so it was not possible to separate the weak emission of the two forms. The maximum of emission in methanol is observed at 320 nm (Figure 1). The emission band extends its blue tail up to 500 nm, suggesting a very weak emission around 450 nm and probably originating from the open structure. However, we failed to isolate this blue emission band. Further experiments are in progress to detect this emission by use of time-resolved emission spectroscopy. The very low emission quantum yield is due to the involvement of bond breaking and twisting processes and mixing of n,π^* and π,π^* excitations at the S_1 state, as supported by the theoretical data of this work. The excitation spectrum of the main emission band shows a structured shape similar to that of the absorption one. However, the small difference in the relative peaks intensities suggests the involvement of an efficient nonradiative process at higher energy of excitation. It may also suggest the existence of several conformers at the ground state, besides a strong solvation due to the polar and H-bonding effects of solvent methanol solution. Both suggestions agree with the theoretical data (vide infra). Note also that the emission band is not a mirror image of the absorption (excitation) spectrum, in agreement with the above suggestions. Finally, relaxation to the ground state might occur via intersystem crossing, with a possible involvement of triplet state(s), and internal conversion to the ground states of the formed isomers through bond breaking, twisting, and H-atom transfer (see theoretical sections).

^{1}H and ^{13}C NMR studies confirm the existence of equilibrium between the two forms (Figure 2). In the ^{1}H NMR spectrum of AB in $CDCl_3$ at 298 K the broadening of some signals prevents an unambiguous identification of both isomers. They are clearly separated at 273 K in an 89:11 ratio (Figure 2a). The ^{13}C{^{1}H} NMR spectrum (298 K) also confirms the presence of both forms (see Figure 2b). The assignment of the resonances was made using information obtained from ^{1}H−^{13}C COSY and NOE spectra.[22] The major isomer corresponds to the ring structure, and the ratio of the two structures changes slightly with the temperature and the solvent, although the ring form is always the most stable structure. The existence of equilibrium between both forms follows from the following points: (i) a saturation transfer between the methyl resonance of both isomers was found when the NOE spectra were reordered; (ii) an increase in the temperature of the $CDCl_3$ solution from 273 K gives rise to a broadening of the resonances.

Previous NMR studies were limited to the observation of both species in DMSO-d_6 at room temperature,[6] and calculations of equilibrium constants were based on the averaged values of chemical shifts estimated from the expected ones of the separated species.[7] To our knowledge, our study is the first temperature-dependent NMR experiment that gives relevant information about energetic and kinetic parameters. Therefore, 1,1′,2,2′-tetrachloroethane-d_2 was chosen as solvent because its high boiling point allows a heating of the sample to 413 K. The two methyl signals of both isomers, observed separately at

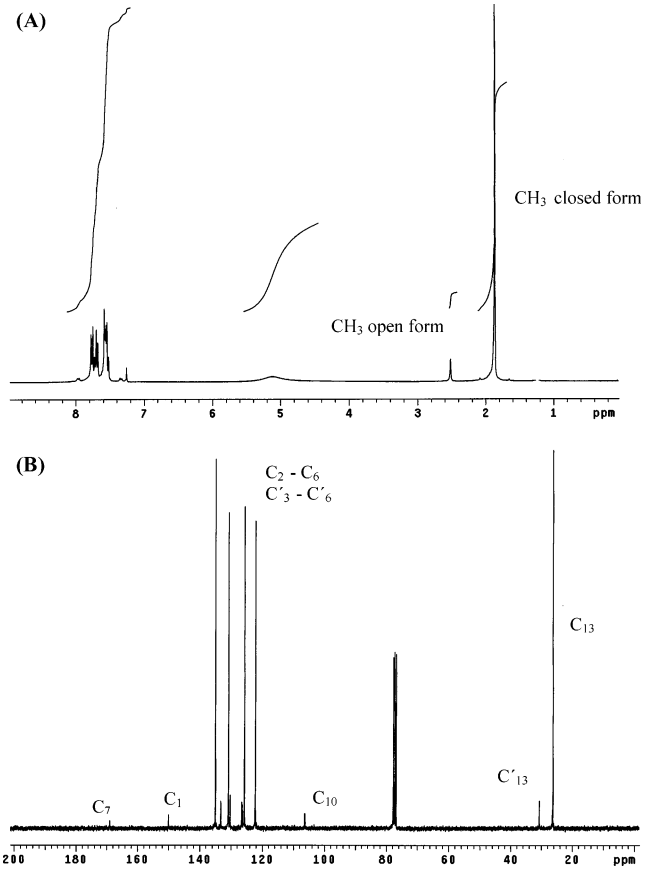

Figure 2. (a) Aromatic part of ^{1}H NMR (300 MHz, 273 K) spectrum of AB in $CDCl_3$. (b) Aromatic part of ^{13}C NMR (300 MHz, 298 K) spectrum of AB in $CDCl_3$. The carbon atom numeration is that used in Scheme 1.

room temperature, broadened as the temperature increased. The coalescence was achieved at $T_c = 380$ K. Because the signals come from different populations, the calculation of the free energy of activation was made using the Shanan-Atidi and Bar-Eli method.[23] Using the coalescence temperature (T_c), the relative population of both signals (P_O = population of the open form, P_R = population of the ring form), and their difference in chemical shift expressed ($\delta\nu$), the rate constants ($k_{R\rightarrow O}$) for the ring → open and ($k_{O\rightarrow R}$) open → ring transformations could be obtained (Table 1). Finally, the Gibbs free energies of activation for both transformations were also calculated using the thermodynamic formulation of the transition state theory.[23]

3.2. Theoretical Results. We will divide this section in two parts. The first one is devoted to the electronic ground state (S_0), where we are mainly interested in the mechanism. The second one deals with the first singlet excited electronic state (S_1), where we are also interested in the mechanism of the ring−chain tautomerism.

Electronic Ground State. The results for the ground state are depicted in Figure 3 where the geometries of the stationary points are shown along with a scheme of their relative energies. The related data are presented in Tables 2 and 3. The most stable

TABLE 2: Values of Potential (V) and Free ($G°$) Energies Relative to Those of R″ Structure and of Dipole Moments of the Stationary Points Located at the Ground Electronic State S_0

parameter	R″	TS_1″	O_1″	TS_2″	O_2″	TS_3″	O_3″
V (gas phase)[a]	0.0	40.6	3.7	17.2	3.8	9.3	3.4
$G°$ (gas phase)[b]	0.0	38.2	2.1	13.5	1.0	6.9	0.5
$G°$ (condensed phase)[b]	0.0	31.8	1.4	10.2	0.6	6.2	0.8
μ (gas phase)[c]	7.9	8.71	7.42	6.43	4.85	3.0	2.17
μ (condensed phase)[c]	6.92	11.91	9.73	8.87	6.43	4.30	3.09

[a] Relative potential energy in kcal/mol. [b] Relative Gibbs free energy in kcal/mol. [c] Total dipole moment in debyes.

TABLE 3: Selected Geometric Parameters of the Stationary Points Located at the Ground Electronic Potential Energy Surface[a]

parameter	R″ [d]	TS_1″	O_1″	TS_2″	O_2″	TS_3″	O_3″
r(7,9)[b]	1.37 (1.36)	1.29	1.33	1.39	1.35	1.35	1.36
r(9,10)[b]	1.46 (1.42)	2.40	3.18	3.11	3.08	3.08	2.73
r(10,11)[b]	1.40 (1.38)	1.30	1.23	1.22	1.22	1.22	1.22
r(11,12)[b]	0.97 (0.95)	1.00	1.62	3.69	3.31	3.12	4.25
r(9,11)[b]	2.34 (2.29)	2.44	2.58	2.78	2.85	2.87	3.41
r(9,12)[b]	2.53 (2.47)	1.80	0.99	0.97	0.98	0.98	0.98
α(1−2−10−11)[c]	119.3 (114.5)	61.1	25.8	18.2	23.7	52.8	124.9
α(2−1−7−9)[c]	−0.5 (−1.4)	−2.4	−31.7	55.8	54.9	−54.9	−15.6
α(1−7−9−12)[c]	36.4 (31.2)	31.8	9.9	82.9	181.7	178.4	180.0

[a] The numeration of the atoms is that of Scheme 1. [b] Interatomic distance in angstroms. [c] Dihedral angle in degrees. [d] Numbers in parentheses refer to the CASSCF optimization.

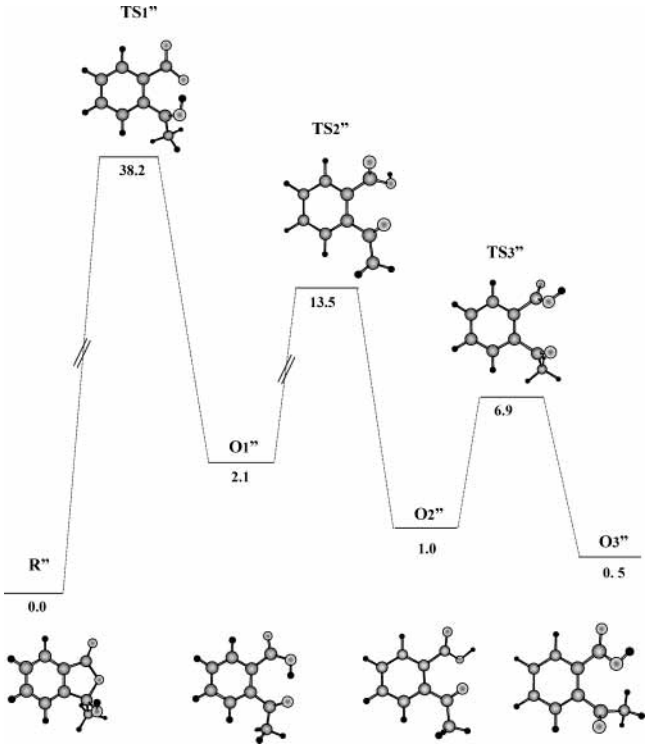

Figure 3. Schematic free energy ($G°$) profiles for the ring−chain tautomerism of AB at the S_0 state. The values of $G°$ (kcal/mol) are relative to that of R″ taken as a reference.

structure in the ground state (for clarity, the ground state structures are labeled by X″, while those of the S_1 state are labeled by X′) corresponds to the closed form called R″ (we will use this nomenclature from now on). The other three minima shown in Figure 3 correspond to isomers of the open form and are called O_1″, O_2″, and O_3″. The last is the more stable one of the open structures in the gas phase, although the energy difference between the three isomers is quite small (Table 2). Three transition states are also depicted in Figure 3, TS_1″, TS_2″, and TS_3″. As explained in the methodological section, IRCs and full optimizations have been carried out in order to ascertain the connection between the minima through each transition state. These connections are indicated by dotted lines in Figure 3. The first transition state TS_1″ connects the closed R″ structure with the first open tautomer O_1″. The other two transition states TS_2″ and TS_3″ correspond to the isomerization of O_1″ toward O_2″ and O_2″ toward O_3″, respectively. We have also found an isomer of the R″ structure corresponding to an internal rotation of the $C_{10}-O_{11}H$ bond. As this structure is higher in energy and it is not directly connected with the cyclization and proton transfer process, we have omitted it in Figure 3 for clarity. Therefore, the whole process shown in Figure 3 corresponds to the formation of the more stable open isomer (O_3″) starting from the more stable closed (R″) form of 2-acetylbenzoic acid.

The values of the energies of the whole process are presented in Table 2, and are relative to that of the more stable R″ form. The potential energy values of the structures shown in Figure 3 are given in the first row of Table 2, whereas the second row includes all the thermodynamic corrections that give the Gibbs free energy ($G°$) according to the formalism outlined in the methodological section. Inclusion of thermodynamic parameters does not greatly modify the energies. The only relevant point is that in terms of $G°$ all the open forms are stabilized by 1−3 kcal/mol. This is mainly due to the entropic term that clearly favors the more disordered open structures with respect to the closed isomer. The third row of Table 2 gives the free energy of the structures when adding the bulk effect of the solvent through the IPCM cavity method. The dielectric constant of

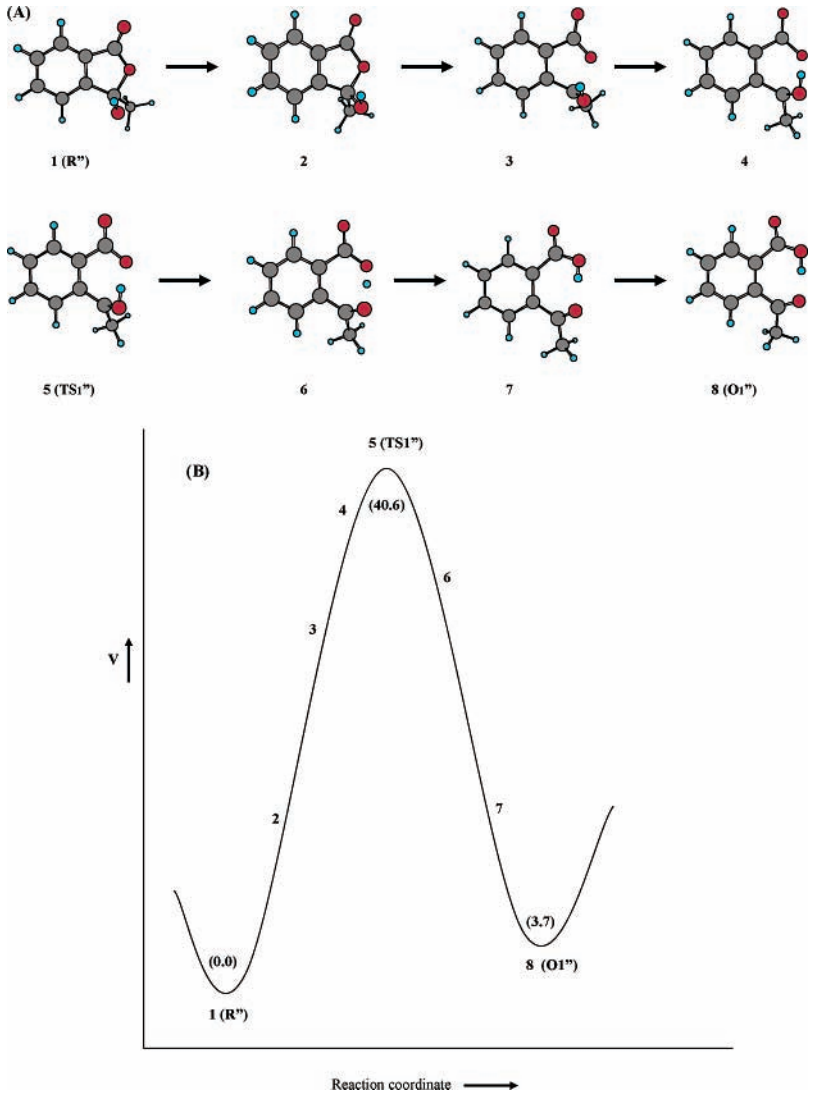

Figure 4. (a) Snapshots of selected geometries along the IRC R″ → TS_1″ → O_1″ at S_0. (b) Relative positions of the potential energy (*V*) of selected points along the whole IRC energy profile at S_0. The numbers in parentheses are those of *V* (kcal/mol) relative to that of R″.

water has been used for these calculations. Note that the solvent greatly diminishes the energy barrier for the ring−chain tautomerism. Also, the open structures suffer an additional lowering with the exception of O_3″, the more stable one in the gas phase, which is slightly destabilized. As a consequence, in water the more stable open form is no longer O_3″ but O_2″, although the differences are not significant (0.2 kcal/mol), and if geometry optimizations were carried out within the cavity method it is quite possible that the ordering would be reversed again.

The last two rows in Table 2 give the dipole moment value of the structures at each stationary point in both the gas and condensed phases. As expected, in the condensed phase the dipole moments are larger as solvent polarizes the system (R″ is an exception). The relative stabilization of the structures upon solvation is correlated with the dipole moment of each structure. This is in fact the case when comparing the different open structures so that the smaller stabilization of O_3″ correlates with the smallest dipole moment values of this isomer. The large lowering of the TS_1″ energy is also accounted for by the large dipole moment of this structure. However, R″, which has a quite large dipole moment value, is almost the less stabilized structure. An explanation of this abnormal behavior can be found in the fact that the closed form is less able to be solvated than the open ones. The molecular frame of the latter structure extends over a larger portion of the space so that more interactions with external (solvating) molecules are possible.

The structures of the stationary points are depicted in Figure 3. The quantitative values of some selected geometric parameters of these points are given in Table 3. In particular, the table gives the values of the distances between the atoms that are directly involved in the cyclization and the proton transfer reaction along with some dihedral angle values that help to understand the internal rotations taking place in the interconversion of the different open structures. The most interesting process is the one that goes from R″ to O_1″ (Figure 3). In this step both the breaking of the bond between the oxygen-9 and the carbon-10 and the proton transfer (hydrogen-12 is transferred from oxygen-11 to oxygen-9) occur in a concerted way. However, the two processes are not simultaneous. This process was further analyzed with the help of the IRC calculations. The IRC starts from the transition structure TS_1″ and goes in the reactant side toward R″ and in the product side toward O_1″ (Figure 4a, Table 3). Even if the reaction in the IRC scheme begins at the transition state, it is easy to understand the process considering the reactant structure as the starting point and with the IRC followed in the reverse sense up to the transition state. At this point the other half of the IRC toward products can be followed in a direct manner. At the early steps of the reaction the relevant motion implies the cleavage of the O_9-C_{10} bond so that at the

transition state (TS) this bond is totally broken (the O_9-C_{10} distance is 2.40 Å at the TS). This breaking is accompanied by a rotation of the C_2-C_{10} bond so that the transferring hydrogen-12 gets closer to the accepting oxygen-9 (Table 3). At this point the system has reached the transition state where all the energy climb was done, and all the way is energetically downhill to O_1'' (Figure 4b). This second part of the reaction almost exclusively involves the motion of the hydrogen atom that is transferred (snapshots 6 and 7 in Figure 4a). Additionally, the O_9-C_{10} angle rotates a little further, and the C_1-C_7 bond slightly turns to reach the minimum energy conformation of the product, O_1''. Figure 4b shows in a pictorial way the relative potential energy (V) position of the selected points of the IRC.

Prior to the analysis of the rest of the reactions, it is interesting to consider the charges of the transferring hydrogen atom and the acceptor and donor oxygen atoms along the R″ to O_1'' process. The Mulliken analysis shows that the transferring hydrogen atom has a positive charge of 0.480 au in R″ which increases slightly along the whole path, passing through the transition state TS_1'' (0.523 au) and ending up in the product O_1'' (0.553 au). As for the charges on the oxygen atoms, they are clearly negative and range between −0.3 and −0.6 au. The oxygen atom directly bounded to the hydrogen is always the more negative one. Therefore, the relative order reverses along the path (it has already reversed in the transition state). At this point it is of interest to discuss the nature of the transfer (i.e., whether it is a proton or hydrogen atom transfer). Given the asynchrony of the transfer, in the transition state the O_9-C_{10} bond is almost broken whereas the H_{12} atom is still bonded to the O_{11} atom. Keeping in mind that our theoretical procedure excludes open-shell structures, this means that the transition state should be a zwitterionic species with a negative charge in the carboxylate fragment and a positive charge on the C_{10} atom. In fact, the analysis of charges reveals an important increment of negative charge in the carboxylate ($C_7O_8O_9$) fragment by −0.559 au, while the positive charge on the C_{10} atom increases only slightly from +0.067 to +0.099 au. However, it should be noted that the positive charge can be delocalized through the π system of the benzene ring as well as to the O_{11} atom. This fact is partially taken into account by considering the global charge of all the atoms directly bonded to C_{10}. The calculation reveals an increment of positive charge of 0.418 au between the R″ and TS_1'' structures. Once the transition state has been reached, the reaction proceeds by the transfer of a proton so that globally a hydrogen atom transfer takes place along the whole reaction coordinate.

The subsequent reactions that transform the open structure O_1'' to the progressively more stable O_2'' and O_3'' rotamers can be easily traced by changes in the dihedral angle values shown in Table 3. In this way the process that starts from O_1'' to O_2'' mostly involves a rotation of the C_7-O_9 bond (that is, the conformation of the hydroxyl group bonded to C_7 is changed; see Figure 4). In addition to that, there is also a significant change of the dihedral angle that involves rotation around the C_1-C_7 bond. Thus, this reaction involves a global reorganization of the COOH group. In the following step that goes from O_2'' to O_3'' the C_1-C_7 bond rotates again, but now in the reverse sense ending at a value quite similar to the one of the initial conformer (O_1''). However, the main component of this step involves motion of the $CO(CH_3)$ group that rotates almost 90° in order to adopt the conformation yielding the final O_3'' product.

Let us compare now these theoretical results with the experimental data reported above. Our NMR spectra at 273 K confirm the existence of the two forms with a ratio of 89:11 in favor of the closed structure. The predominance of the closed one is, in fact, a general trend of all the reported works,[6,7] and it is also consistent with our theoretical results. The closed form R″ lies below O_3'', the more stable open isomer in the gas phase. In terms of $\Delta G°$, the difference is quite small: 0.5 kcal/mol (0.8 kcal/mol in the condensed phase, where the O_2 structure is the more stable open isomer). Larger differences of free energy would imply a very small relative population of the less stable species, unable to be detected.

On the other hand, dynamic NMR experiments have allowed the measurement of the kinetics and energetics of this ring−chain tautomerism (Table 1). The reported values of $\Delta G°^{\#}_{(R\rightarrow O)} = 19$ kcal/mol for the direct (closed to open form) reaction and $\Delta G°^{\#}_{(O\rightarrow R)} = 18$ kcal/mol for the reverse one imply that both forms are separated by 1 kcal/mol in terms of $\Delta G°$. The calculated difference in free energy in the condensed phase of 0.8 kcal/mol between both tautomers (R″ and O_3'') (Table 2) fits very well with the experimental one (1 kcal/mol). Results in Table 2 also allow a direct comparison with the NMR kinetic data. The higher transition state (TS_1'') found along the whole reaction path implies energy barriers (in terms of $G°$ and in the condensed phase) of 31.8 and 31.0 kcal/mol for the direct and reverse processes, respectively. In this case the agreement with experiment is only qualitative. Inclusion of the solvent effect greatly diminishes the Gibbs free energy of the transition state. If optimization of the geometry in condensed phase were allowed, a further decrease of the energy barrier would probably show up. Note that theoretical calculations of the Gibbs free energy barrier are subject to quite drastic model approximations such as the use of the harmonic oscillator and the rigid rotor for the vibrational and rotational degrees of freedom of the molecule, respectively. Also, the condensed phase is introduced through an (approximate) continuum model that only takes into account the effect of the solvent molecules as a bulk. Finally, the values of the energetics and kinetics parameters deduced from the experiments are also subject to the approximations of the thermodynamic formulation of the transition state theory, the Shanan-Atidi and Bar-Eli Method,[22] and supposition of only two equilibrated structures: open and ring forms.

First Singlet Excited Electronic State. Before analyzing the potential energy curves obtained for the first singlet excited electronic state (S_1), it is important to know the exact nature of the electronic transition. As there are no symmetry elements along the whole reaction path, we have always followed the first excited state irrespective of the nature of the excitation.

For the S_1 closed structure, the electronic excitation is almost exclusively constituted by the HOMO−LUMO π,π^* transition. Figure 5a depicts the shape of these orbitals. While the HOMO is mainly a π orbital of the benzene ring, the LUMO has some nonnegligible contribution from the remaining heavy atoms. In particular, the LUMO presents significant contributions from C_7, O_9, and O_{11} atoms. The description of the excited state arising from the open form (O_3'') is, however, more complicated as there are three orbitals involved in the excitation which could be described as a combination of the HOMO−LUMO and the (HOMO-2)−LUMO excitations. These are depicted in Figure 5b. The HOMO and LUMO orbitals are qualitatively similar to the ones described for the closed tautomer, although clear differences in the contributions of the atomic orbitals are observed when both figures are compared. The shape of the other involved orbital, the HOMO-2, is different. It seems to be mainly due to a lone electron pair located at the oxygen-11. In this case the usual belief that n and π orbitals do not mix does not apply. The reason for that lies in the particular geometry

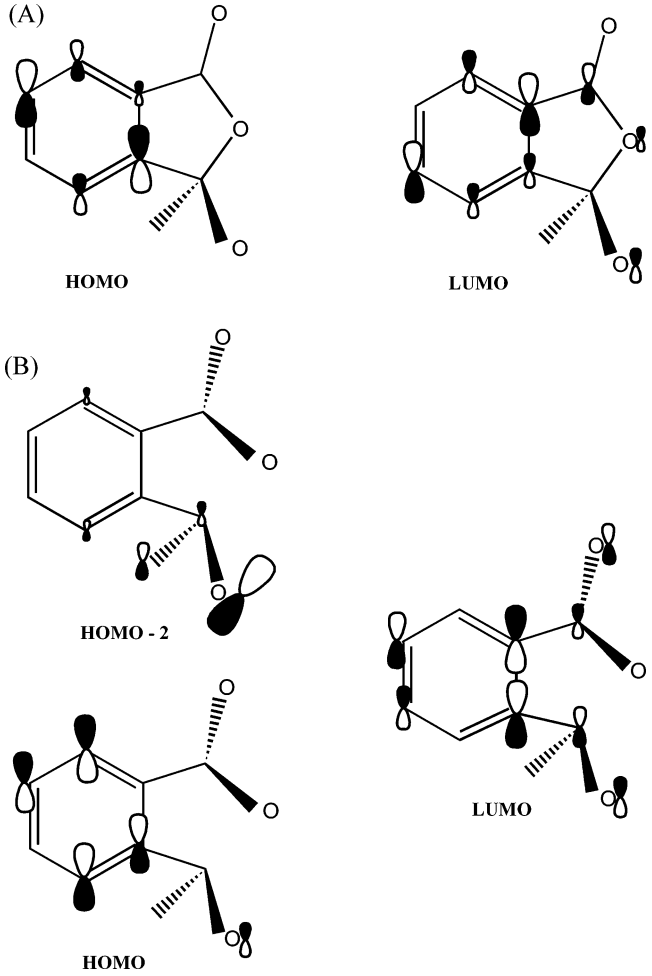

Figure 5. (A) Shape of orbitals involved in $S_0 \rightarrow S_1$ electronic excitation for the closed form (R″). (B) Shape of orbitals involved in $S_0 \rightarrow S_1$ electronic excitation for the open form (O_3″).

of the open isomer. As we are considering here the most stable conformer O_3″ in gas phase, this conformer presents the $CO(CH_3)$ fragment lying in a plane almost perpendicular to the benzene ring (see Figure 3 and Table 3). Thus, the lone pair n orbitals of the oxygen atom in the carbonyl group are not both orthogonal to the π system of the benzene ring: one of them is located in almost the same plane. Therefore, the excited state now is not π, π^* or n, π^* but a mixing of both. The mixing of these states and the involvement of cyclization and proton transfer explain the lower emission quantum yield of AB in solution, as said above. The shape of these orbitals can also explain the main differences, both geometric and energetic, observed between the ground and the excited electronic states.

For the excited state S_1, we have carried out the same kind of calculations performed for the ground state. As explained in the methodological section, we have used the CIS method to explore the potential energy surface at S_1. As the CIS energies may be subject to errors,[24] we have recalculated the energy of the stationary points by using the TD-DFT method within the B3LYP functional.[15] This method is quite recent, but it has already been proved to give much more accurate results for intramolecular proton transfer reactions, comparable in some cases to the ones obtained with the very computing demanding CASPT2 method.[25] Results are shown schematically in Figure 6, where the different stationary points and the reaction paths linking them are shown. The actual values of the relative potential energies and dipole moments of each structures are given in Table 4. Some selected geometric parameters (inter-

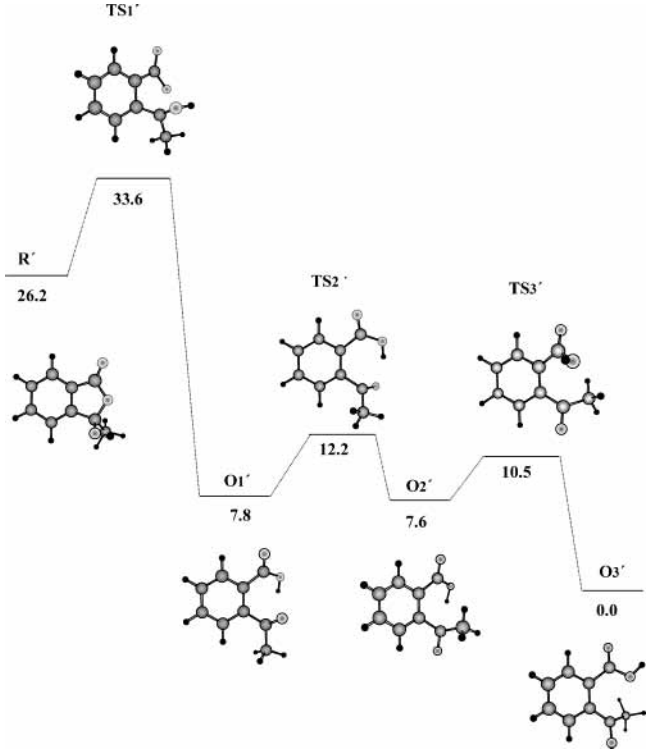

Figure 6. Schematic potential energy (V, in kcal/mol) profile for ring−chain tautomerism of AB at the S_1 state. The indicated values are those of V relative to that of O_3′.

atomic distances and dihedral angles) of the stationary points are given in Table 5.

One well-known drawback of CIS and TD-DFT methods is their inability to treat double and multiple excitations. This problem can be avoided using the more flexible CASSCF method. To see whether this problem is affecting our result, we have performed CASSCF calculations on the reactant (ring form). The active space considered included 12 electrons and 11 orbitals (six occupied and five virtual), so all the π system and the highest σ and lowest σ^* orbitals are considered. The σ orbital roughly corresponds to a lone pair of the oxygen-9, whereas the σ^* is predominantly $C_{10}-O_9$ antibonding. With this quite large system we have optimized the geometry of the reactant in both S_0 and S_1 electronic states. The obtained geometries are posted in Tables 3 and 5 so we can compare them with the DFT and CIS results, respectively. At the S_0 level, there are small differences. However, at S_1 the CIS and CASSCF geometries are almost equal. We have also analyzed the CAS wave function to ascertain that double excitations have a very small contribution to the whole wave function which is mainly constituted, as in the CIS case, by the HOMO−LUMO single excitation. We have also tried to localize the transition state at the CASSCF level for the S_1 state. However, the optimization was unsuccessful because the orbitals made sudden changes along the optimization so that following a coherent active space proved fruitless. In any case, analysis of the CASSCF wave function at fixed (CIS) geometry also reveals a main contribution of single excitations. There is also an important contribution from the HOMO-1 → LUMO excitation, a fact that is also present in the TD-DFT calculation. This probably indicates a crossing of π orbitals along the reaction coordinate. In any case, the contributions of double (and higher) excitations to the CASSCF S_1 wave function are very small, so a diradical character of the process seems to be excluded.

Figure 6 reveals a general shape of the energy profile quite similar to the one of the ground state depicted in Figure 3. The

TABLE 4: Potential Energies and Dipole Moment Values of the Stationary Points Located in the First Singlet Excited Electronic State S_1

parameter	R′	TS_1′	O_1′	TS_2′	O_2′	TS_3′	O_3′
V(CIS)[a]	20.0	47.6	4.5	7.2	3.6	11.6	0.0
Δ*E*(CIS)[b]	131.87	107.26	96.28	98.75	93.69	103.99	104.14
V(TD-DFT)[a]	26.2	33.6	7.8	12.16	7.63	10.52	0.0
Δ*E*(TD-DFT)[b]	107.17	75.73	73.11	77.20	71.65	73.71	75.28
V (condensed phase)[a]	14.2	38.0	2.4	5.9	2.4	1.0	0.0
μ (gas phase)[c]	1.09	2.38	4.35	6.50	6.93	7.35	5.4
μ (condensed phase)[c]	1.50	3.20	5.60	8.34	9.02	10.39	7.55

[a] Relative potential energy in kcal/mol. [b] Difference in energy between S_0 and S_1. [c] Total dipole moment in debyes.

TABLE 5: Selected Geometric Parameters of the Stationary Points Located in the First Singlet Excited Electronic State Potential Energy Surface[a]

parameter	R′ [d]	TS_1′	O_1′	TS_2′	O_2′	TS_3′	O_3′
r(7,9)[b]	1.36 (1.36)	1.29	1.33	1.32	1.33	1.36	1.33
r(9,10)[b]	1.42 (1.42)	1.94	3.01	2.98	2.94	2.92	2.90
r(10,11)[b]	1.38 (1.38)	1.34	1.26	1.26	1.26	1.26	1.26
r(11,12)[b]	0.95 (0.95)	0.95	2.49	1.96	3.11	4.29	4.75
r(9,11)[b]	2.29 (2.29)	2.44	2.84	2.87	3.92	3.93	3.90
r(9,12)[b]	2.45 (2.46)	2.39	0.95	0.95	0.95	0.95	0.95
α(1−2−10−11)[c]	115.1 (112.7)	64.1	39.5	−68.8	−152.3	−158.3	−156.3
α(2−1−7−9)[c]	1.7 (1.5)	3.1	36.8	17.5	32.7	28.6	28.1
α(1−7−9−12)[c]	23.0 (29.1)	44.8	−6.1	1.2	−1.0	86.5	176.8

[a] The numeration of the atoms is that adopted in Scheme 1. [b] Interatomic distance in angstroms. [c] Dihedral angle in degrees. [d] Numbers in parentheses refer to the CASSCF optimization.

closed form R′ undergoes a hydrogen atom transfer reaction and a bond-breaking process so that open tautomers are formed. Analysis of Mulliken charges along the whole process reveals the same pattern observed for the ground state. The charge of the hydrogen is almost constant as it goes from +0.50 to +0.49 au from R′ to O_1′ with an irrelevant increase to +0.53 au at the transition state TS_1′. A charge analysis similar to the one performed for the ground electronic state reveals also patterns similar to the ones discussed before, although now an important fraction of the charge separation produced by the heterolytic cleavage of the O_9-C_{10} bond in the transition state tends to concentrate in the benzene ring rather than in the carboxylate and C_{10} fragments. In this way the increment of negative charge of the $C_7O_8O_9$ carboxylate fragment is −0.288 au, whereas the increase of positive charge of the fragment including C_{10} and neighboring atoms is only +0.148 au, but for instance, the charge on C_1 (in the phenyl ring) changes from −0.403 to +0.201 au.

At this point some comments about the validity of the TD-DFT method to deal with proton transfer reactions are in order. In a very recent contribution,[26] the TD-DFT method has been successfully used for the study of excited state reactivity problems, at least when the geometries were optimized at the CASSCF level. Another recent work has shown that, when the ground state is well described by DFT methods (such as in our case), the TD-DFT excited state description is comparable to that obtained in ground state DFT calculations.[27] Given that in the case presented here CIS and CASSCF geometries are very similar, we believe that our theoretical procedure is giving quite reliable results for the system considered here. An important drawback of the TD-DFT method, recently described, is that it systematically underestimates the energy of charge transfer excited states.[28] This comes from the very weak overlap between the orbitals involved in the charge transfer transition so that a local functional can hardly have an effect on the excitation energy. The use of hybrid functionals which include nonlocal Hartree−Fock exchange, such as the B3LYP method used here, is expected to lead to more reliable results. In fact, we are not dealing with a charge transfer excited state, so this problem is not greatly affecting our results. It may be that the first transition state TS_1′ is too stabilized at the TD-DFT level (as it has noticeable charge separations although it is not actually a charge transfer state as previously discussed). This would only mean that the energy barrier for the first process will be slightly higher than the value reported in Table 4 and Figure 6 (7.4 kcal/mol).

Depending on the internal rotations of the −COOH and $-CO(CH_3)$ groups, AB progressively passes from the initial O_1′ tautomer to O_2′ and O_3′ forms, each one being more stable than the previous structure. However, a more careful analysis reveals some differences from the S_0 results. The minima (stable structures) and the transition states connecting them are different. This is clearly seen by looking at the actual values posted in Table 4 (and comparing them with the ones corresponding to S_0 given in Table 2). The first row in Table 4 gives the potential energy values obtained with the CIS calculations whereas the third row contains the values recalculated with the TD-DFT method at fixed geometry. There are no qualitative differences between both levels of calculation, although some quantitative differences are worth noting. At both levels of calculations the closed R′ structure is no longer the more stable one as the O_3′ structure has a clearly lower energy. This inversion of the stability of tautomers upon electronic excitation has been observed in many related systems.[29] The first transition state that connects the closed R′ structure with the first open

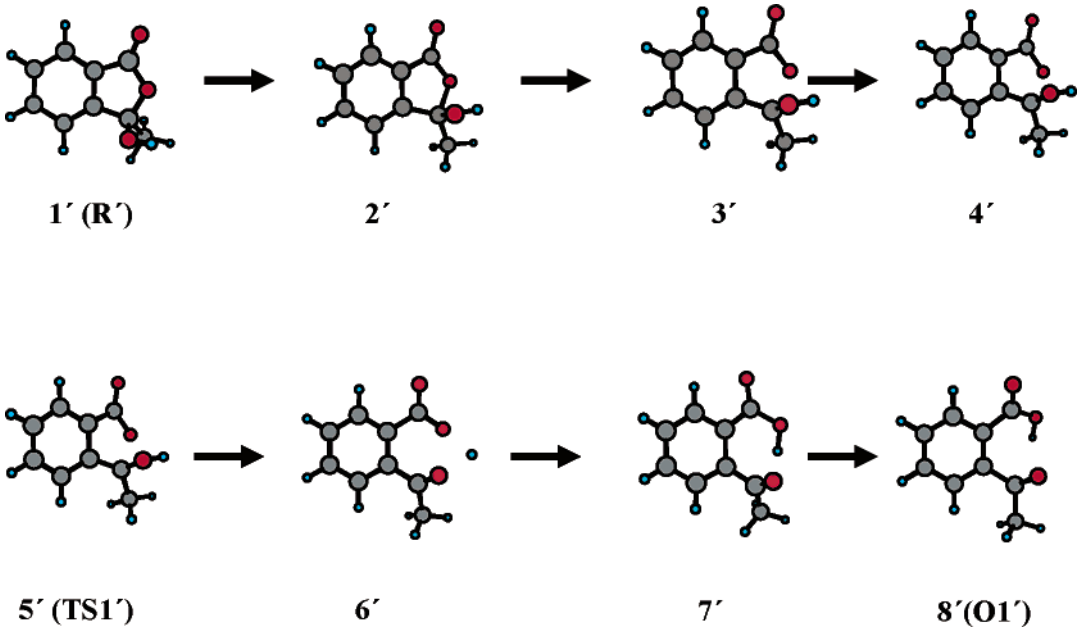

Figure 7. Snapshots of selected geometries along calculated IRC R′ → TS_1′ → O_1′ for the S_1 excited state.

conformer O_1′ is the higher point in energy along the path. TD-DFT clearly lowers this barrier, which is only 7.4 kcal/mol. In any case, TD-DFT does not modify the fact that this is the highest energy point along the whole reaction path. As for the rest of the path, it consists of internal rotations of the −COOH and −CO(CH_3) groups, as noted above. Energetically, the gaps are now larger than the corresponding ones in the ground state (compare again results in Tables 2 and 4). As discussed above, the TD-DFT energy barrier for R′ → O_1′ is probably too small, but the CIS value is too high because it is well-known that the CIS method tends to overestimate the barriers for the proton transfer reactions.[24] As explained, we have been unable to localize the transition state at the CASSCF level but a single CASSCF calculation upon CIS optimized structures gives an energy barrier of 28.0 kcal/mol, quite close to the CIS value (27.6 kcal/mol). Of course, introduction of dynamic correlation (a CASPT2 calculation, for instance) would certainly lower this value[25c] so that the actual energy barrier is expected to lie between 8 and 25 kcal/ mol.

We have also analyzed the reaction path that goes from R′ to O_1′ at the excited state in order to see whether the breaking of the cycle and the H-atom transfer processes are taking place simultaneously. The IRC calculations reveal that the whole process in S_1 is qualitatively very similar to the one in S_0. This fact is pictorially demonstrated in Figure 7, where the geometries of some selected points along the IRC are presented so that a direct visual comparison with the same reaction in S_0 can be done (Figure 4a).

The bulk effect of a polar solvent (dielectric constant of water) has also been considered at S_1. Corrections of the CIS energies with the solvent effect are given in the third row of Table 4. Again, there are no significant differences, so the relative ordering of energies is maintained. All the relative energies are lowered. This means that upon solvation the reference O_3′ structure is the less stabilized one. Total dipole moments values in the gas phase and in the condensed phase are given in the last two rows of Table 4. The loose relationship between solvent stabilization and the dipole moment values observed in the ground state no longer applies at S_1. This suggests that higher electric moments (quadrupole, octupole, ...) may play a major role at S_1. The closed R′ structure is now largely stabilized upon solvation even if it has the lowest dipole moment among the values reported in Table 4. Note that in the ground state the closed R″ structure has one of the largest dipole moments but it was almost the less stabilized structure. In any case, the fact that solvent does not significantly affect the energy profile for the H-atom transfer and ring-breaking process is an additional proof of the process not being zwitterionic (this also applies to the ground state results previously analyzed). This fact also validates the TD-DFT/CIS strategy as erroneous descriptions of the excited state (not taking into account double excitations) would bias the calculation toward zwitterionic transition states.

Other interesting data to discuss here are the excitation energies along the PES. The differences in energies between S_0 and S_1 at the stationary points of S_1 are given in Table 4 in kilocalories per mole at both the CIS and TD-DFT levels (second and fourth rows). Note that excitation energies are always quite high and that they do not change abruptly along the different regions of the PES where the stationary points are found. CIS excitation energies are higher (always above 90 kcal/mol) and those from TD-DFT slightly lower, but even there the excitation energy is never less than 70 kcal/mol. Besides, these high values are also maintained along the different sections of the calculated IRC. These results then clearly demonstrate that there are no intersections between the ground and excited states, at least not near the lower energy zones of the PES, the only ones of chemical interest. To compare the theoretical excitation energies with the experimental absorption and fluorescence spectra, data in Table 4 are not useful as they give the differences in energy at the stationary points of S_1, whereas the absorption process takes place from the minimum energy structures of the ground state S_0. The vertical transition absorption band from the most stable closed tautomer is calculated to appear at 247 nm at the TD-DFT level. On the other hand, the adiabatic 0−0 transition is predicted at 260 nm if the zero point energy is assumed to be equal in both electronic states. These results are to be compared with the CASSCF calculations which predict the bands of the vertical and adiabatic transitions at 259 and 273 nm, respectively. All these values are in quite good agreement with the experimentally observed absorption maximum found at 278−282 nm. As for the absorption of the most stable open form O_3″, which could be

in equilibrium with the closed tautomer in the ground state, the Franck−Condon vertical transition is calculated at 308 nm within the TD-DFT method.

Less evident is the comparison of the fluorescence spectrum with our excitation energies because it is not known where along the whole path (proton transfer + ring opening + internal rotations) the system comes back to the ground state. Given that the open forms have the lower energy, it is reasonable to assume that electronic deactivation proceeds from the open isomers; the energy range for light emission should correspond to the electronic excitations of the open forms that lie around 70−80 kcal/mol. This corresponds to wavelengths ranging between 360 and 410 nm, again in a reasonable agreement with the experimental fluorescence spectra shown in Figure 1. Note that our theoretical results are for isolated molecules (i.e., gas phase), whereas the emission spectra are obtained in solution. Therefore, part of the discrepancy between computed and observed bands might be attributed to the solvent effect on both ground and excited state potential energy surfaces and on solvent-dependent emission quantum yield.

To end the description and discussion of results at S_1, let us now consider a few geometric parameters of the stationary points posted in Table 5. As at S_0, the first step at S_1 is the one involving the proton transfer and the opening of the pyrrolic cycle. Both processes take place in a concerted way (that is, in a single kinetic step), but they are not synchronous. An enlargement of the O_9-C_{10} distance takes place in the first stages of the reaction so that in the transition state the bond is almost broken. Interestingly, the O_9-C_{10} distance in TS_1' is clearly shorter than the one in TS_1''. However, this difference in both states can be solely attributed to the fact that in S_1 the transition state occurs earlier than in S_0 because the reactant has higher energy than the product, and so the Hammond postulate applies.[30] Once the transition state TS_1' has been reached, the reaction path proceeds to the transfer of hydrogen-12. The energy goes down monotonically, and the first open tautomer O_1' is reached. The rest of the reaction path can be followed by checking the dihedral parameters given in Table 5. From O_1' to O_2' structure, the C_2-C_{10} bond turns upside down (the dihedral angle changes almost 180°), whereas the final step that transforms O_2' in the final O_3' product involves also a whole 180° turn of the O−H group (indicated by the 1−7−9−12 dihedral angle in Table 5). In parallel with the S_0 results, we have found additional transition state structures that correspond to different internal rotations of the open tautomer. Because they are not directly involved in the process that goes from the closed R′ structure to the more stable open tautomer O_3', they are not posted in Figure 6.

4. Conclusions

In this paper we have presented experimental and theoretical results that help to understand the complex mechanism involved in the ring−chain tautomerism of 2-acetylbenzoic acid at both S_0 and S_1 states.

From the experimental side, our results clearly show the existence of an equilibrium between the ring and open forms, the ring one being clearly predominant (~90%). The emission quantum yield is very weak, in agreement with the theoretical data showing a mixing between π,π^* and n,π^* states, and the involvement of proton transfer and cyclization processes. Electronic calculations have also disclosed the presence of several conformers of the open form. The one directly linked to the ring tautomer, O_1'', is not the most stable one, O_3''. To obtain O_3'' from O_1'', two steps are necessary that involve an additional conformer O_2'' and two transition states that correspond to internal rotations of the −COOH and $-CO(CH_3)$ fragments. We have also analyzed the IRC for the tautomerization process. Both H-atom transfer and ring breaking/formation are occurring in a concerted but not synchronous manner.

In the first singlet excited electronic state S_1, the whole energy profile is qualitatively similar to the S_0 one. However, the more stable tautomer at S_1 is not the ring form but one of the open conformers O_3'. The energy barrier for the ring−chain tautomerism is 7.4 kcal/mol at our best level of calculation (TD-DFT). The vertical excitation structure is found 5.8 kcal/mol above the minimum at the TD-DFT level. Therefore, the ring−chain tautomerism can be considerably enhanced upon irradiation at the appropriate wavelength. This opens the door to potential applications of proton transfer and ring−chain tautomerism in different fields of science and technology such as photochromism and for building materials able to store information at the molecular level and for controlling structural changes in supramolecular environments by using ultrafast (i.e., femtochemistry) techniques.

Finally, we have found that solvent does not greatly affect the gas phase results. The energy profiles obtained from gas phase electronic calculations are qualitatively similar to the condensed phase ones even if the dipole moments may change considerably along the involved reactions.

Acknowledgment. We are grateful for financial support from the Spanish Ministerio de Ciencia y Tecnología through Project Nos. MAT-2002-01829 and BQU2002-00301, the JCCM (PAI-02-004), the Fondo Europeo de Desarrollo Regional, the use of the computational facilities of the CESCA, and the computational service of the Universidad de Castilla-La Mancha.

References and Notes

(1) (a) Caldin, E. F.; Gold, V. *Proton-Transfer Reactions*; Chapman and Hall: London, 1975. (b) Douhal, A.; Lahmani, F.; Zewail, A. H. *Chem. Phys.* **1996**, *207*, 477 and references therein. (c) *Hydrogen Transfer: Experiment and Theory*; Limbach, H., Manz, J., Eds.; *Ber. Bunsen-Ges. Phys. Chem.* **1998**, *102*.

(2) (a) Jones, P. R. *Chem. Rev.* **1963**, *53*, 461. (b) Valters, R. E.; Flitsch, W. *Ring Chain Tautomerism*; Plenum Press: New York, 1985.

(3) Bowden, K. *Chem. Soc. Rev.* **1995**, 431.

(4) Bowden, K. *Organic Reactivity: Physical and Biological Aspects*; Golding, B. T., Griffin, R. J., Maskill, H., Eds.; Royal Society of Chemistry: Cambridge, 1995; p 123.

(5) Felker, P. M.; Lambert, W. R.; Zewail, A. H. *J. Chem. Phys.* **1982**, *77*, 1603.

(6) Finkelstein, J.; Williams, T.; Toome, V.; Traiman, S. *J. Org. Chem.* **1967**, *32*, 3229.

(7) (a) Bowden, K.; Taylor, R. G. *J. Chem. Soc B* **1971**, 1390. (b) Bowden, K.; Taylor, R. G. *J. Chem. Soc B* **1971**, 1395. (c) Bowden, K.; Henry, M. P. *J. Chem. Soc., Perkin Trans. 2* **1972**, 201. (d) Bowden, K.; Henry, M. P. *J. Chem. Soc., Perkin Trans. 2* **1972**, 206. (e) Bowden, K.; Malik, F. P. *J. Chem. Soc., Perkin Trans. 2* **1993**, 635. (f) Bowden, K.; Byrne, J. M. *J. Chem. Soc., Perkin Trans. 2* **1996**, 1921. (g) Bowden, K.; Byrne, J. M. *J. Chem. Soc., Perkin Trans. 2* **1997**, 123. (h) Bowden, K.; Hiscocks, S. P.; Perjessy, A. *J. Chem. Soc., Perkin Trans. 2* **1998**, 291. (i) Bowden, K.; Raja, J. *J. Chem. Soc., Perkin Trans. 2* **1999**, 39. (j) Bowden, K.; Misic-Vukovic, M. M.; Ranson, R. J. *Collect. Czech. Chem. Commun.* **1999**, *64*, 1601.

(8) Dobson, A. J.; Gerkin, R. E. *Acta Crystallogr., Part C* **1996**, *C52*, 3078.

(9) (a) Skrinarova, Z.; Bowden, K.; Fabian, W. M. F. *Chem. Phys. Lett.* **2000**, *316*, 531. (b) Fabian, W. M. F.; Bowden, K. *Eur. J. Org. Chem.* **2001**, 303.

(10) (a) Humbert, B.; Alnot, M.; Quilès, F. *Spectrochim. Acta, Part A* **1998**, *54*, 465. (b) Sobolewski, A. L.; Domcke, W. *Chem. Phys.* **1998**, *232*, 257. (c) Maheshwari, S.; Chowdhury, A., Sathyamurthy, N.; Mishra, H.; Tripathi, H. B.; Panda, M.; Chandrasekhar, J. *J. Phys. Chem. A* **1999**, *203*, 6257.

(11) Frisch, M. J.; Trucks, G. W.; Schlegel, H. B.; Scuseria, G. E.; Robb, M. A.; Cheeseman, J. R.; Zakrzewski, V. G.; Montgomery, J. A.; Stratmann,

R. E.; Burant, J. C.; Dapprich, S.; Millam J. M.; Daniels, A. D.; Kudin, K. N.; Strain, M. C.; Farkas, O.; Tomasi, J.; Barone, V.; Cossi, M.; Cammi, R.; Menucci, B.; Pomelli, C.; Adamo, C.; Clifford, S.; Ochterski, J.; Petersson, G. A.; Ayala, P. Y.; Cui, Q.; Morokuma, K.; Malick, D. K.; Rabuck, A. D.; Raghavachari, K.; Foresman, J. B.; Ciolowski, J.; Ortiz, J. V.; Stefanov, B. B.; Liu G.; Liashenko, A.; Piskorz, P.; Komaroni, I.; Gomperts, R.; Martin, R. L.; Fox, D. J.; Keith, T.; Al-Laham, M. A.; Peng, C. Y.; Nanayakkara, A.; Gonzalez, C.; Challacombe, M.; Gill, P. M. W.; Johnson, B. G.; Chen, W.; Wong, M. W.; Andrés, J. L.; Head-Gordon, M.; Replogle, E. S.; Pople, J. A. *Gaussian 98*; Gaussian Inc.: Pittsburgh, PA, 1998.

(12) (a) Becke, A. D. *J. Chem. Phys*. **1993**, *98*, 5648. (b) Becke, A. D. *J. Chem. Phys*. **1992**, *96*, 2155.

(13) Lee, C.; Yang, W.; Parr, R. G. *Phys. Rev. B* **1988**, *37*, 785.

(14) Foresman, J. B.; Head-Gordon, M.; Pople, J. A.; Frisch, M. J. *J. Phys. Chem*. **1992**, *96*, 135.

(15) Gordon, M. S. *J. Phys. Chem.* **1996**, *100*, 3974.

(16) (a) Ditchfield, R.; Hehre, W. J.; Pople, J. A. *J. Chem. Phys*. **1971**, *54*, 724. (b) Ditchfield, R.; Hehre, W. J.; Pople, J. A. *J. Chem. Phys*. **1972**, *56*, 2257. (c) Hariharan, P. C.; Pople, J. A. *Mol. Phys.* **1974**, *27*, 209. (d) Gordon, M. S. *Chem. Phys. Lett*. **1980**, *76*, 163. (e) Clark, T.; Chandrasekhar, J.; Spitznagel, G. W.; Schleyer, P. v. R. *J. Comput. Chem*. **1983**, *4*, 294.

(17) (a) Hegarty, D.; Robb, M. A. *Mol. Phys.* **1979**, *38*, 1795. (b) Ross, B. O.; Taylor, P. R.; Siegbahn, P. E. M. *Chem. Phys.* **1980**, *48*, 157.

(18) Schlegel, H. B. *J. Comput. Chem*. **1982**, *3*, 214.

(19) Gonzalez, C.; Schlegel, H. B. *J. Chem. Phys*. **1989**, *90*, 2154.

(20) McQuarrie, A. D. *Statistical Thermodynamics*; University Science Books: Mill Valley, CA, 1973.

(21) Foresman, J. B.; Keinth, T. A.; Wiberg, K. B.; Snoonian, J.; Frisch, M. J. *J. Phys. Chem*. **1996**, *100*, 16098.

(22) Pretsch, E.; Bühlmann, P.; Affolter, C. *Structure Determination of Organic Compounds*; Springer Verlag: Berlin, 2000.

(23) Sandström, J. *Dynamic NMR Spectroscopy*; Academic Press: London, 1982.

(24) (a) Scheiner, S. J. *Phys. Chem. A* **2000**, *104*, 5898. (b) Casadesús, R.; Moreno, M.; Lluch, J. M. *Chem. Phys.* **2003**, *290*, 319.

(25) (a) Andersson, K.; Malmqvist, P.-Å.; Roos, B. O.; Sadlej, A. J.; Wolinski, K. *J. Phys. Chem.* **1990**, *94*, 5483. (b) Andersson, K.; Malmqvist, P.-Å.; Roos, B. O.; Sadlej, A. J.; Wolinski, K. *J. Phys. Chem.* **1992**, *96*, 1218. (c) Vendrell, O.; Moreno, M.; Lluch, J. M. *J. Chem. Phys.* **2002**, *117*, 7525.

(26) Fantacci, S.; Migani, A.; Olivucci, M. *J. Phys. Chem. A* **2004**, *108*, 1208

(27) (a) Furche, F.; Ahlrichs, R. *J. Chem. Phys.* **2002**, *117*, 7433. (b) Wanko, M.; Garavelli, M.; Bernardi, F.; Niehaus, T. A.; Frauenheim, T.; Elstner, M. *J. Chem. Phys.* **2004**, *120*, 1674.

(28) (a) Sobolewski, A. L.; Domcke, W. *Chem. Phys.* **2003**, *294*, 73. (b) Dreuw, A.; Weisman, J. L.; Head-Gordon, M. *J. Chem. Phys.* **2003**, *119*, 2943.

(29) (a) Organero, J. A.; Douhal, A.; Santos, L.; Martínez-Ataz, E.; Guallar, V.; Moreno, M.; Lluch, J. M. *J. Phys. Chem. A* **1999**, *103*, 5301. (b) Organero, J. A.; Moreno, M.; Santos, L.; Lluch, J. M., Douhal, A. *J. Phys. Chem. A* **2000**, *104*, 8424. (c) Casadesús, R.; Moreno, M.; Lluch, J. M. *Chem. Phys. Lett.* **2002**, *356*, 423.

(30) Hammond, G. S. *J. Am. Chem. Soc.* **1955**, *77*, 334.